Proceedings of GT2006
2006 ASME Turbo Expo: Power for Land, Sea, and Air
May 8-11, 2006, Barcelona, Spain

GT2006-91098

IMPACT OF MANUFACTURING VARIABILITY ON COMBUSTOR LINER DURABILITY

Sean Bradshaw
Department of Aeronautics and Astronautics
Massachusetts Institute of Technology
77 Massachusetts Avenue
Cambridge, Massachusetts 02139
Email: sdbrad@mit.edu

Ian Waitz
Department of Aeronautics and Astronautics
Massachusetts Institute of Technology
77 Massachusetts Avenue
Cambridge, Massachusetts 02139
Email: iaw@mit.edu

ABSTRACT

This paper presents a physics-based, probabilistic model that quantifies the impact of manufacturing variability on the cup-to-cup and engine-to-engine variations of combustor liner temperature and Low Cycle Fatigue (LCF) life. This probabilistic model is applied to a gas turbine engine combustor for a commercial aircraft. The model is assessed using combustor liner wall temperature measurements and combustor outlet gas temperature measurements. A Monte Carlo analysis shows that this model estimates cup-to-cup combustor outlet temperature variations and liner wall temperature variations consistent with these measurements. Furthermore, this analysis indicates that approximately 90 percent of the combustors designed to the calculated life using deterministic methods will most likely fail earlier than predicted. A sensitivity analysis identifies the thermal barrier coating (TBC) surface emissivity as the key driver of the minimum liner life for a combustor where the radiative loads in the primary zone far exceed the convection loads. Reducing the variability of the TBC surface emissivity by 90 percent yields a minimum liner life increase of seven percent of the nominal liner life. However, these results are dependent on the accuracy of the model and on the levels of manufacturing variability assumed for the input parameters. Other design parameters are shown to drive combustor liner life for combustor where the radiative loads are comparable to the convective loads.

Keywords: combustor, heat transfer, durability, variability

NOMENCLATURE

$\chi =$ random variable
$\mu =$ mean value
$\sigma =$ standard deviation
$V =$ coefficient of variation
$\beta =$ beta distribution
$G =$ mass flow conductance
$\dot{m} =$ mass flow rate
$\rho =$ density
$\Delta P =$ liner pressure drop
$\Psi_M =$ dome air mass flow surrogate
$\Delta_M =$ cooling hole mass flow surrogate
$I =$ total current
$e =$ voltage potential
$\phi =$ equivalence ratio
$f =$ fuel-air ratio
$T =$ temperature
$PF =$ profile factor
$U =$ velocity
$\zeta =$ turbulent mixing parameter
$\bar{\sigma} =$ Stefan-Boltzmann constant
$L =$ length
$t =$ thickness
$\dot{q} =$ liner heat flux
$h =$ convection heat transfer coefficient
$\varepsilon =$ emissivity
$\alpha =$ absorptivity

$k =$ thermal conductivity
$\hat{L} =$ flame luminosity factor
$F =$ view factor
$A =$ area
$\eta =$ film effectivness
$B =$ blowing ratio
$s =$ slot height
$N_f =$ LCF life
$a =$ crack length
$H =$ crack growth rate correction factor
$K =$ stress intensity factor
$\hat{Y} =$ standard response surface equation output
$\hat{\sigma} =$ stress
$l_b =$ mean beam length
$d_h =$ metering hole diameter

1 Introduction

The lifetime of a gas turbine combustor is typically limited by the durability of its liner, the structure that surrounds the hot combustion gases and anchors the flame (Figure 1). The primary objective of the thermal design process for a gas turbine combustor is to ensure that liner temperatures do not exceed a maximum design temperature limit consistent with the combustor life requirements, while minimizing the amount of film cooling air used in the process. Combustor liner temperatures that exceed the maximum design temperature during flight operations can increase thermally-induced LCF, leading to cracking and buckling of the liner [1] (Figure 2). This design temperature is set by metallurgical limits of the nickel-based alloys used to construct the liner.

Accurate estimation of combustor liner life requires a combination of empirical correlations, high fidelity numerical models, and rig testing. This process can take several months to complete. Furthermore, geometrical and aerothermal variability arising from imperfect manufacturing processes introduce uncertainty to the deterministic quantification of combustor liner life. In addition, the computational expense of the numerical tools used to estimate combustor liner life prohibit the use of probabilistic methods. As a result, the effects of manufacturing variability are typically accounted for by making conservative assumptions and adopting design margins based on experience with similar products. However, using design margins does not necessarily lead to optimized combustor configurations in the presence of manufacturing variability. Identification and mitigation of the manufacturing variability sources that significantly impact the mean and variance of combustor liner life is necessary in order to achieve a robust design.

Although there are several papers that focus on design with variability for gas turbine engines [3–5] and more broadly in fields other than gas turbine engines, there is little work reported on this area for gas turbine combustors. Mavris and Roth [6] introduced a general robust design methodology for the High Speed Civil Transport (HSCT) impingement-cooled combustor liner. They used a finite element model in order to estimate the liner thermal loads deterministically. Using Design of Experiments (DoE) techniques, they assembled a response surface equation (RSE) for liner temperature as a function of several design parameters. The flame temperature, the film cooling air temperature, and the hot-side convection coefficient were classified as noise parameters. Mavris and Roth showed that impingement hole spacing and the thermal barrier coating (TBC) thickness were the key drivers of liner temperature variance. The authors modeled the variability of the hot-side convection coefficient, the compressor discharge temperature, and the adiabatic flame temperature using triangular probability density functions, where the first and second moment characteristics were based on design experience. The triangular distribution was chosen because the true natures of the probability distributions for these parameters were not known.

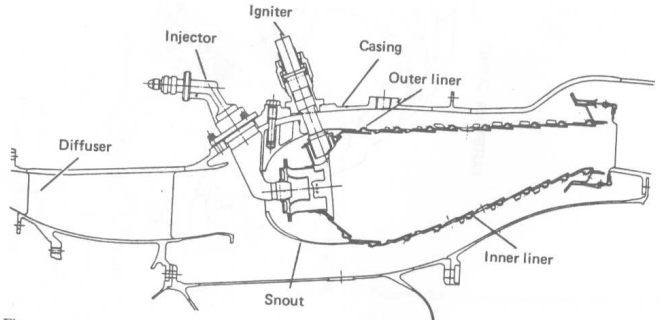

Figure 1. Combustor cutaway

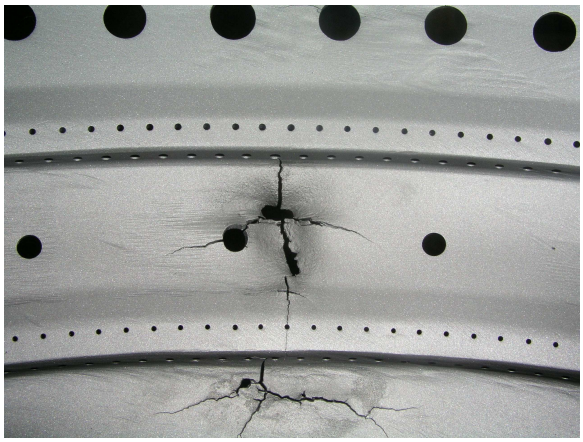

Figure 2. Combustor liner distress: cracking and burn-throughs (*courtesy of Delta Airlines)*

2 Scope of Paper

This paper presents a probabilistic modeling methodology for estimating the impact of manufacturing variability on combustor liner LCF life (Section 3). This model enables causal relationships to be established among key design parameters, their tolerances, and liner life in a probabilistic manner. We have also directly assessed this model to allow us to assert its validity (Section 4). We have performed this assessment using combustor rig data obtained during the final development of the combustor as well as data obtained during the subsequent use of the combustor in the field. Furthermore, we have demonstrated a fundamental mean shift in the combustor liner life distribution as a result of manufacturing variations (Section 5). Finally, we have applied a one-at-a-time sensitivity analysis in order to identify the key drivers of combustor liner LCF life (Section 6).

3 Probabilistic Model Overview

The probabilistic model presented in this paper is a simplified, physics-based model relating the impact of manufacturing variability to liner temperature and LCF life for a gas turbine combustor used on a commercial aircraft. This combustor liner, which consists of N fuel injectors and five liner panels, has several annular slots for the injection of film cooling air axially along flame side of the liner surface. The liner temperature and LCF life are estimated for a high temperature region downstream of the film cooling slots.

An overview of the analytical architecture is shown in Figure 3. The probabilistic model consists of four main parts: a manufacturing variability model, a network flow model, a 1-D heat transfer model, and a combustor liner life model. The latter three models were calibrated using higher fidelity simulations of the combustor flow field, the liner temperatures, and the liner stresses. A Monte Carlo analysis was used to propagate the effects of manufacturing variability through a simplified combustor LCF life model in order to estimate the resulting combustor LCF life probability distribution for a fleet of engines. This analysis was performed using MATLAB. The CHEMKIN 3.7 software package was used to model the thermodynamics and chemical kinetics of the combustor flow field. The Monte Carlo analysis consisted of 10,000 trials. During the process of developing this model, many choices had to be made in order to balance practicality versus fidelity. These choices are described in greater detail in the following sections.

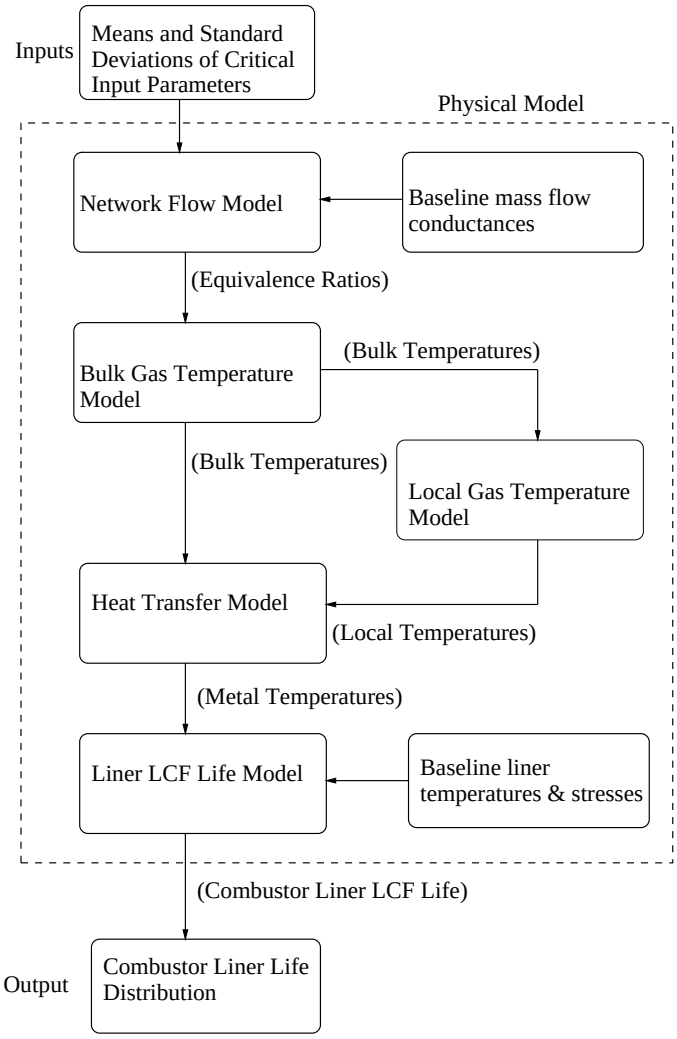

Figure 3. Probabilistic model overview

3.1 Manufacturing Variability Modeling

The gas turbine combustor manufacturing process produces variability in the part dimensions and some thermo-physical parameters. For the combustor analyzed in this paper, we modeled the variability of the metering hole diameter, the cooling slot height, the TBC emissivity, the TBC thickness, the liner thickness, the bond coat thickness, the TBC thermal conductivity, the liner thermal conductivity, the bond coat thermal conductivity, the dome flow rate, the fuel injector mass flow rate, and the outlet temperature variability factor. The first eleven parameters are modeled as independent, normally distributed random variables as shown in Equation 1. The mean values (μ_{χ_i}) and the standard deviations (σ_{χ_i}) of these parameters (χ_i) are based on the nominal design values and manufacturing tolerances, respectively. The manufacturing tolerances are assumed to determine the variability of these parameters with 95 percent confidence or to within plus or minus two standard deviations of the nominal values. The manufacturing tolerances are taken from part drawings and other design specifications. The twelveth parameter, the near wall gas temperature profile factor, is a noise variable that is modeled as a standard Beta distribution. In Equation 2, the Beta distribution

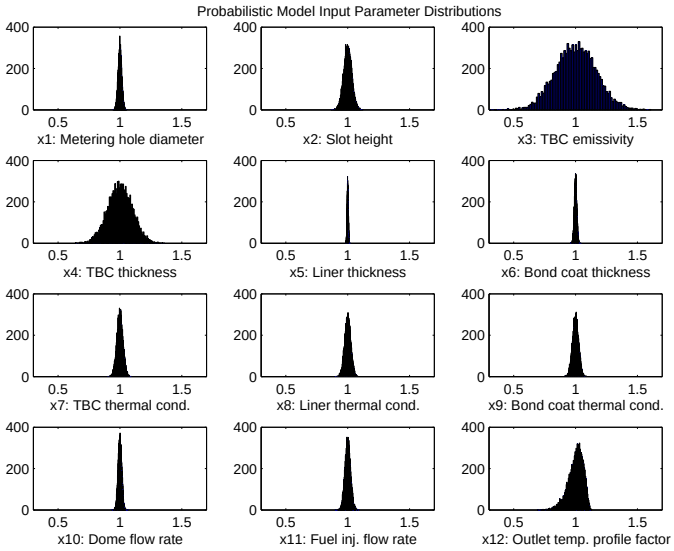

Figure 4. Probabilistic model input parameters

parameters q_β and r_β are determined by specifying the mean and variance and then solving Equations 3 and 4 simultaneously.

$$\chi_i \sim N(\mu_{\chi_i}, \sigma^2_{\chi_i}) \tag{1}$$

$$\chi_{12} \sim \beta_{\chi_{12}}(q_\beta, r_\beta) \tag{2}$$

$$\mu_{\chi_{12}} = \frac{q_\beta}{q_\beta + r_\beta} \tag{3}$$

$$\sigma_{\chi_{12}}{}^2 = \frac{q_\beta r_\beta}{(q_\beta + r_\beta)^2 (q_\beta + r_\beta + 1)} \tag{4}$$

The means and variances of the first 11 parameters have been normalized by their mean values (Equation 5) and plotted in Figure 4. V_{χ_i} is the coefficient of variation of the parameter χ_i. The outlet gas temperature profile factor distribution has been normalized by its mean value in Figure 4. These histograms show that the TBC emissivity, the TBC thickness, and the combustor outlet temperature profile factor have the three highest percent variation.

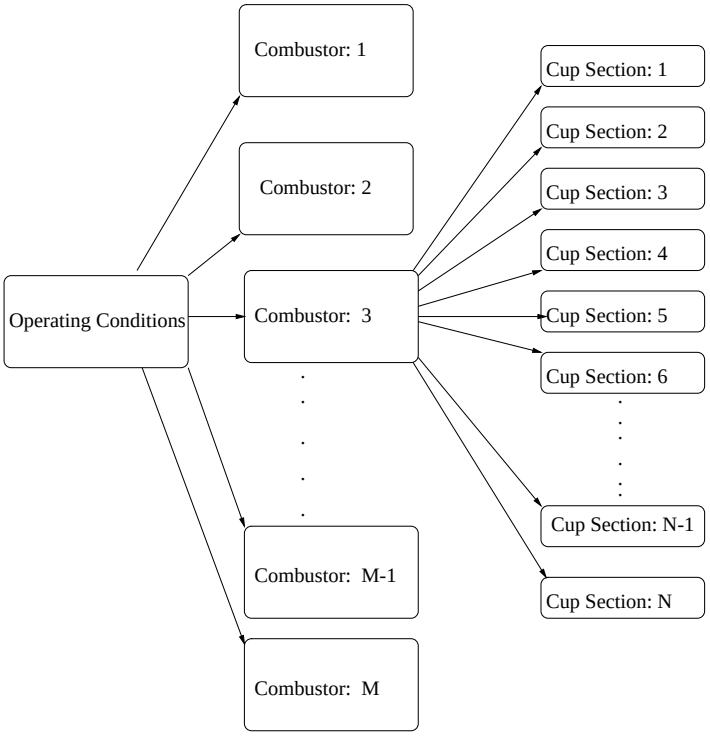

Figure 5. Variability nesting diagram for 'M' combustors and 'N' cup sections

$$\chi_i \sim N(1, V_{\chi_i}{}^2) \tag{5}$$

The combustor is divided into N circumferential cup sections corresponding to N fuel injectors for this probabilistic analysis. Some parameters vary from cup to cup within a combustor while others vary from combustor to combustor. Cup-to-cup variations are caused by manufacturing variations which are apparent from cup section to cup section within a single combustor. For example, the air mass flow rate and the fuel injector mass flow rate exhibit variability from cup to cup. As a result, the equivalence ratios and bulk gas temperatures vary from cup to cup. Engine-to-engine variations are due to manufacturing variations apparent from combustor to combustor. The liner, TBC, and bond coat thicknesses thermal conductivities, the slot height, the metering hole diameter, and the TBC wall emissivity predominantly vary from combustor to combustor for the fabrication process associated with the design we have studied. The cup-to-cup variability that exists for these parameters is much smaller than the engine-to-engine variations. Thus, these parameters are modeled solely as engine-to-engine variations. As a result, it is necessary to model these variations in a nested fashion when performing a probabilistic analysis. Figure 5 provides an overview

of the framework for modeling manufacturing variability in gas turbine combustors. The liner life will differ in the presence of manufacturing variability for two combustors that operate under the same external conditions.

The construction of a probabilistic combustor simulation requires that these nested levels of variability are carefully accounted for. The first step is to assemble the dome areas one cup at a time in order to model the cup-to-cup variability of the fuel injector and dome air mass flow rates. The second step is to propagate the variations in the fuel injector mass flow rate and the swirler mass flow rate via a network flow model in order to determine the impact of these variations on the bulk gas equivalence ratio for each axial panel station for a combustor with N cup sections. Third, the bulk gas temperature model propagates the equivalence ratio variability to the bulk gas temperature. The first of these models, a network flow model, is presented in the next section.

3.2 Network Flow Model

The combustor network flow model estimates the cup-to-cup variability of the bulk gas mass flow rate. The network model propagates the variability of the mass flow conductances while enforcing the conservation of mass for a combustor annulus consisting of N cup sections.

The network flow model has the following assumptions:

1. Mass is conserved.
2. The fuel injector mass flow rate is negligible.
3. The flow across the combustor liner is modeled as incompressible.
4. The burner pressure is constant; pressure gradients inside the burner are negligible.
5. The total combustor outlet mass flow rate is constant.
6. There is no mixing in the circumferential direction between adjacent cup section flows.
7. The blockage effects of the fuel-injector struts are neglected.
8. The dilution air mixes instantaneously with the bulk flow over each panel.
9. The cooling film flow mixes with the next downstream panel section bulk flow.

The combustor network model is composed of a linear circuit with parallel conductances corresponding with the mass flow capacities across the air admission holes. A current source is used to model the effect of a constant mass flow rate through the combustor. The circuit branch currents model the mass flow rates through the air admission holes. The nominal equivalent mass flow conductances for the dome, the cooling film, and the dilution air for each panel are based the design mass flow distribution for the combustor under consideration. This network flow model is solved using the node method.

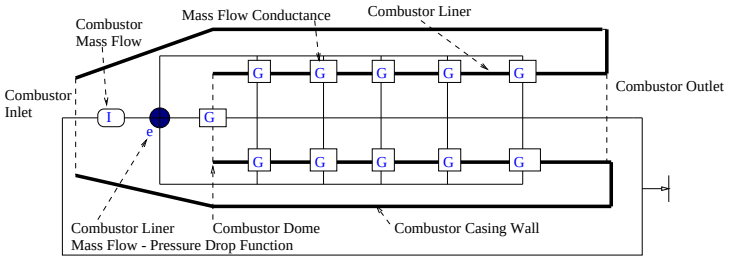

Figure 6. Combustor network flow model: electrical domain

The total mass flow rate and the nominal pressure drop across the combustor liner are known a priori from combustor rig tests. Thus, the first step in the solution process is to estimate the equivalent mass flow conductance, G^o_{eq}, of the combustor using data for the combustor mass flow rate, $\dot{m}_c$, the film cooling air density, ρ_{cool}, and the known nominal combustor liner pressure drop, ΔP_{nom}, in Equation 6.

$$G^o_{eq} = \frac{\dot{m}_c}{\sqrt{2\rho_{cool}\Delta P_{nom}}} \tag{6}$$

Once the equivalent mass flow conductance for the combustor has been computed, then the nominal mass flow conductances, G^o_i, for the circuit are determined by multiplying the known percent mass flow conductances through the air admission holes by the nominal equivalent conductance as shown in Equation 7.

$$\frac{G^o_i}{G^o_{eq}} = \frac{\dot{m}_i}{m_c} \tag{7}$$

The mass flow conductances for film cooling holes and the dilution holes for the combustor we studied do not vary significantly from cup-to-cup within this combustor. Thus, for a single combustor, the dome air mass flow conductances are the only random variables. The nominal dome air mass flow conductance for each cup section is multiplied by samples from the parameter, Ψ_M, which is assumed to be normally distributed with unity mean and with a variance determined from the dome air mass flow tolerence in order to simulate the effects of manufacturing variability (Equations 8, 9). σ_{Ψ_M} is based on the swirler mass flow tolerance.

$$\Psi_M \sim N(1, \sigma^2_{\Psi_M}) \tag{8}$$

$$G_i = \Psi_M G_i^o \sim N(G_i^o, G_i^{o2}\sigma^2_{\Psi_M}) \quad (9)$$

The film cooling air mass flow and dilution air mass flow conductances are driven by the metering hole and the dilution hole diameters. These hole diameters are updated simultaneously in the network model for each combustor. The update is executed by multiplying the parameter, Λ_M, by the nominal conductances for these holes. Λ_M is a function of the ratio of the actual metering hole diameter to the nominal metering hole diameter for this combustor as shown in Equation 10. The mechanisms that introduce combustor-to-combustor variability in the metering hole diameters also similarly impact the dilution hole diameters. As result, Λ_M is multiplied by the nominal dilution hole mass flow conductances for each combustor in order to simulate the effects of combustor-to-combustor variability in the network model.

$$\Lambda_M = (\frac{d_h}{d_h^o})^2 \quad (10)$$

$$G_i = \Lambda_M G_i^o \quad (11)$$

The node method is used to solve for the combustor liner mass flow-pressure drop function. First, the equivalent conductance under the presence of variability is estimated by adding the conductances for the cooling film, the dilution air, and the dome flow. Then, the potential difference, e, is computed by dividing the total combustor mass flow rate by the equivalent conductance, $\hat{G}^o_{eq}$ as shown in Equation 12. Finally, the mass flow rate for the i^{th} flow path is computed using Equation 13, where G_i is the i^{th} flow path mass flow conductance and ΔP is the combustor liner pressure drop.

$$e = \frac{I}{\hat{G}^o_{eq}} = \sqrt{2\rho_{cool}\Delta P} \quad (12)$$

$$\dot{m}_i = G_i e = G_i\sqrt{2\rho_{cool}\Delta P} \quad (13)$$

The new equivlent mass flow conductance for a single combustor is determined by computing the equivalent dome air mass flow conductance under the presence of variability and adding it to the effective film cooling air and dilution air mass flow conductances. Applying the node method yields a new combustor pressure drop function consistent with an updated equivalent combustor mass flow conductance due to the dome air flow variability. As a result, the pressure drop for each probabilistic combustor, and therefore, the mass flow for each circuit branch, varies from combustor-to-combustor.

3.3 Bulk Gas Temperature Modeling

After the air mass flow distribution has been determined for each combustor with N cup sections, the fuel mass flow rate is used to estimate the equivalence ratios, ϕ, for each cup section over all 5 panels using Equation 14. This equivalence ratio distribution is subsequently used to estimate the bulk gas temperature, and ultimately, the liner temperature variability, for each combustor. Furthermore, the variabilities of the fuel mass flow rate and the dome air mass flow rate are propagated through Equation 14 in order to yield estimates of the cup-to-cup variation of the equivalence ratios.

$$\phi = \frac{f}{f_{st}} = \frac{\dot{m}_{fuel}/\dot{m}_{bulk}}{f_{st}} \quad (14)$$

The combustion gas temperatures and compositions are determined using adiabatic, well-stirred reactors (WSRs), which are idealized flow systems in which the reactancts are perfectly mixed with the combustion products. Thus, the products have a temperature equivalent to that of the fuel-air mixture inside the WSR chamber. The inputs needed for a well-stirred reactor computation are the equivalence ratio, the residence time, the chamber pressure, and the inlet gas temperature. Estimates of the bulk gas equivalence ratios based on the network flow analysis are used along with the well-stirred reactor model to estimate the bulk gas temperature above each liner panel section.

The WSR model has three main inputs. The inlet gas temperature is the compressor discharge temperature. The chamber pressure is assumed to be the combustor outlet pressure. The residence time is a function of the combustor volume, a reference density, and the combustion gas mass flow rate. In addition, the WSR analysis used in this model assumes that the process is adiabatic. A 20-step, 13-species simplified chemical kinetics mechanism is used to model kerosene-air combustion and solve for the flame temperature [7]. The WSRs models apply the conservation of species and the conservation of energy in order to solve for the mass fractions and flame temperature of the combustion products.

The network flow model requires the solution of M by N WSRs per simulated combustor. Since solving for this many reactors is computationally expensive, a response surface equation relating flame temperature to inlet gas temperature and equiva-

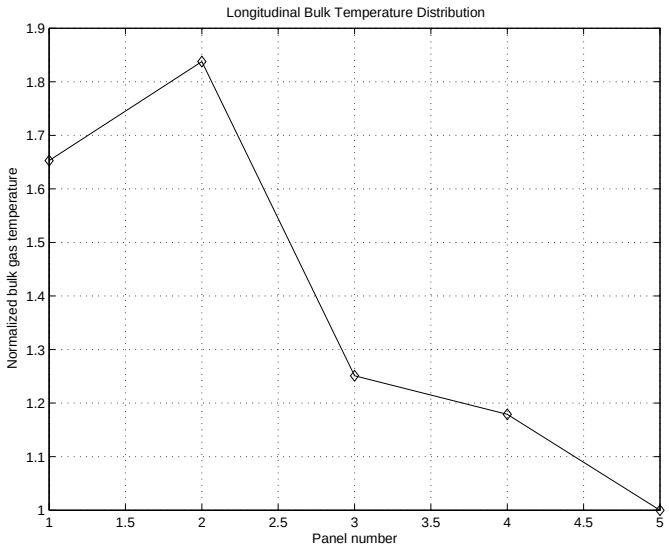

Figure 7. Longitudinal bulk gas temperature distribution

lence ratio at the average combustor residence time was assembled (Equation 15).

$$T_{bulk} = \sum_{n} f_n(T_3)\phi^n \tag{15}$$

The regressors for this polynominal of degree n in ϕ are functions of the combustor inlet temperature, T_3. Thus, for a combustor panel section, specifying the equivalence ratio yields the bulk gas temperature. Cup-to-cup variability in equivalence ratio yields the cup-to-cup variability of bulk gas temperature throughout the combustor, which is used, via a heat transfer model, to estimate the cup-to-cup variability of liner temperature.

A plot of the longitudinal bulk gas temperature rise normalized by the overall combustor temperature rise for each panel station is shown in Figure 7. In the model, the normalized bulk gas temperature increases from 1.65 to 1.84 between panel one and two. Then, normalized the bulk gas temperature steadily decreases from 1.84 to 1.0 between panel 2 and panel 5. The bulk temperature decreases as a result of the mixing process between the combustion products and the cooling air.

3.4 Local Gas Temperature Modeling

Combustor unmixedness, particularly in the combustor primary zone, yields large radial and circumferential variations in the combustion gas temperatures near the wall. This near-wall flow temperature influences the magnitude of the convection load at the liner surface. As a result, the mean and standard deviation of the near-wall gas temperature are modeled in order to yield accurate results when comparing the model's estimate of cup-to-cup liner temperature with the experimental data.

The effects of combustor unmixedness on the local gas temperature are modeled by an empirical combustor gas temperature profile factor in Equation 16. ζ is an empirical turbulent mixing parameter, x_c is distance from the fuel injector, and L_c is the burner length. The mixing rate is calibrated based on the combustor outlet gas temperature profile factor mean and standard deviation. Solving for ζ at $x_c = L_c$ yields an equation for the mixing parameter as a function of the combustor outlet conditions (Equation 17). The combustor outlet gas temperature profile factor, PFt^e, is modeled with Equation 18. The Beta distribution parameters, q_β and r_β, are determined from Equations 3 and 4. The Beta distribution is an appropriate model here for two reasons. First, the outlet temperature variability factor is bounded between zero and one. Second, the mean value of this parameter is near one. As a result, a normal distribution does not satisfy these constraints even for relatively small standard deviations.

$$PF_T = \frac{T_{gas} - T_3}{T_{bulk} - T_3} = 1 - exp(-\zeta \frac{x_c}{L_c}) \tag{16}$$

$$\zeta = -ln(1 - PFt^e)] \tag{17}$$

$$PFt^e \sim \beta(q_\beta, r_\beta) \tag{18}$$

The local gas temperature variability at a panel station is a function of the bulk temperature variability above that panel and the circumferential variability induced by the outlet gas temperature profile factor. The outlet gas temperature variability factor is not a form manufacturing variability. However, the severity of the unmixedness effects modeled by this equation may be affected by manufacturing variability. For modeling purposes, the gas temperature variability factor may be considered as a noise source which acts on the local gas temperature field. This effect may be mitigated in practice by increasing combustor mixedness.

3.5 Radiation Temperature Modeling

The radiation model is based on the assumption of the radiative exchange between a nongray, isothermal gas and a single surface gray enclosure located at the mean beam length [1]. However, steep temperature gradients exist in the combustor primary zone. For example, the near-wall gas temperatures differ

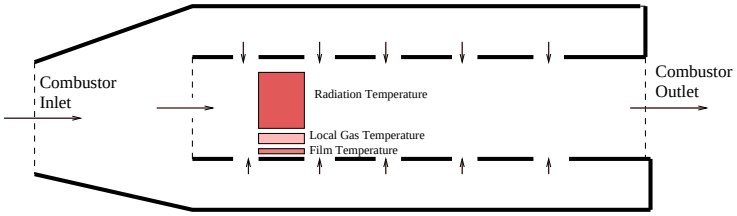

Figure 8. Combustor driving temperatures: radiation temperature, local gas temperature, film temperature

from the average bulk gas temperatures and the centerline bulk gas temperature. Thus, the bulk gas is divided into two driving temperature regions, the effective or global radiation temperature and the near-wall or local gas temperature (Figure 8). The radiation temperature is an artifact of the radiative load being a field property. The radiative heat flux is a function of the gas volume, gas optical depth, direct exchange area, radiating gas emissive power, and surface irradiation [14]. However, the simplest model for the radiative load in combustor thermal design practice is one that uses the effective radiation temperature concept, which is adopted here. Although temperature gradients exist in the combustor, particularly in the primary zone, the model assumes that the temperature field is uniform above a liner panel section. As a result, the effective radiation temperature is set equal to the bulk gas temperature for each liner panel section.

3.6 Heat Transfer Modeling

The combustor liner heat transfer model consists of a steady, one-dimensional heat transfer model that includes radiation, convection, and conduction. The application of a one-dimensional model is appropriate when the temperature gradients in the radial direction are at least an order of magnitude greater than the temperature gradients in the circumferential and axial directions. This is the case for the combustor that we have modeled. The radiative energy transfer to the liner wall is a large fraction of the total liner wall heat flux. This effect is exacerbated in the primary zone, where the combustion gas temperatures are the greatest and the liner walls are in relatively close proximity to the flame. In addition to the liner wall irradiation, convection plays a significant role in setting the liner heat flux. The interaction of hot combustion gases with liner surfaces results in heat transfer from hot gases to the wall. Cooling film flows mitigate this effect somewhat by providing a protective layer between the hot gases and the liner surface. Conduction heat transfer is driven by the temperature gradient between the hot side of the TBC surface and the cold side of the liner. By assuming that the heat transfer process is in steady-state, the heat flux and the TBC, bond coat, and liner temperatures can be estimated using the 1-D heat transfer model shown below [1, 2].

$$\dot{q} = h_f(T_{film} - T_{tbc}) + C_1\bar{\sigma}(\varepsilon_{rad}{T_{rad}}^4 - \alpha_{rad}{T_{tbc}}^4) \tag{19}$$

$$\dot{q} = \frac{k_{tbc}}{t_{tbc}}(T_{tbc} - T_{bnd}) \tag{20}$$

$$\dot{q} = \frac{k_{bnd}}{t_{bnd}}(T_{bnd} - T_{mh}) \tag{21}$$

$$\dot{q} = \frac{k_m}{t_m}(T_{mh} - T_{mc}) \tag{22}$$

$$\dot{q} = h_b(T_{mc} - T_{cool}) + C_2\bar{\sigma}({T_{mc}}^4 - {T_{cool}}^4) \tag{23}$$

$$\eta = \frac{T_{gas} - T_{film}}{T_{gas} - T_{cool}} \tag{24}$$

$$\frac{\alpha_{rad}}{\varepsilon_{rad}} = \left(\frac{T_{rad}}{T_{tbc}}\right)^{1.5} \tag{25}$$

$$\varepsilon_{rad} = 1 - \exp(-28600P_4\hat{L}(fl_b)^{0.5}(T_{rad})^{-1.5}) \tag{26}$$

$$C_1 = \frac{1}{2}(1 + \varepsilon_{tbc}) \tag{27}$$

$$C_2 = \frac{1}{\frac{1-\varepsilon_w}{\varepsilon_w} + \frac{1}{F_{w-c}} + \frac{1-\varepsilon_c}{\varepsilon_c}\frac{A_w}{A_c}} \tag{28}$$

C_1 accounts for the fact that the TBC surface is gray instead of black. Thus, the effective absorptivity of the TBC surface is

accounted for by this constant [1]. The liner and casing walls are modeled as long concentric cylinders with gray surfaces in order to estimate the radiative heat exchange [15] between the liner and the casing. C_2 in Equation 28 quantifies these effects and is a function of the liner emissivity, ε_w, the casing wall emissivity, ε_c, the view factor, F_{w-c}, the liner surface area, A_w, and the casing wall surface area, A_c. $\hat{L}$ is the flame luminosity factor, which accounts for the increased radiosity of the flame as a result of luminous carbon particles in the fuel rich primary zone. For kerosene-air combustion, this factor is set to 1.7 for the bulk flow over panel sections one and two [1]. Otherwise, the flame luminosity factor is set to 1.0 for the rest of the combustor [8].

The film cooling flow impacts the liner convection heat transfer load by altering the near wall film temperature and velocity profiles. The film effectiveness, η, models the effects of the former. This parameter is based on an empirical correlation with the cooling slot height, s, and the blowing ratio, B, as independent parameters. The blowing ratio is defined in Equation 30, where the velocity profile factor, $PF_U = \frac{U_{gas}}{U_{bulk}}$, is the ratio of the near wall gas velocity to the average bulk gas flow velocity [9]. This parameter accounts for the radial velocity gradients in the combustor flow field in order to more accurately estimate the blowing ratio for each liner panel section. The velocity profile factor, which is determined based on CFD calculations of the combustor flow field, is assumed to be constant over each liner panel. In addition, $\dot{m}_{film}$, is the film cooling mass flow rate, A_s, is the cooling slot area for a cup section, A_{bulk}, is the bulk flow-through area.

$$\eta = f(B,s) \tag{29}$$

$$B = \frac{1}{PF_U}\frac{\dot{m}_{film}/A_s}{\dot{m_{bulk}}/A_{bulk}} \tag{30}$$

The hot side convection heat transfer coefficient, h_f, is computed using a Nusselt number correlation which accounts for the impact of the cooling film on the near-wall velocity profile [1]. The back side convection heat transfer coefficient, h_b, is estimated via a Nusselt Number correlation for thermally developing, turbulent pipe flow [10, 15].

This system of equations is solved simultaneously for the heat flux ($\dot{q}$), the TBC temperature (T_{tbc}), bond coat temperature (T_{bnd}), the hot-side liner temperature (T_{mh}), the cold-side liner temperature (T_{mc}), the film temperature (T_{film}), the gas emissivity (ε_{rad}), and the gas absorptivity (α_{rad}) using a Newton-Raphson Method.

3.7 Liner Life Model

Cracking, the primary combustor liner failure mode, is caused by high temperatures and temperature gradients, resulting in high thermal stresses [18]. A combustor liner is considered a "failed" part when either one of two limiting conditions has been exceeded. The first failure condition occurs when a crack initiates and then subsequently propagates longitudinally until it reaches a maximum allowable crack length [19]. The second condition occurs when the stress intensity factor of the liner exceeds the critical stress intensity factor, leading to fast fracture of the part. In order to model these two components of combustor liner LCF life, a crack initiation model and a crack propagation model are used.

The total liner panel section LCF life is computed via Equation 31. N_f is the number of cycles to failure, N_{fi} is the number of cycles to crack initiation, and N_{fp} is the number of cycles until either the crack size reaches some maximum allowable length or the stress intensity factor reaches a critical value. The combustor LCF life is equal to the mininum LCF life of the set of computed LCF lives for all of the panel sections.

$$N_f = N_{fi} + N_{fp} \tag{31}$$

The crack initiation model is based on a proprietary polynomial equation which relates the number of cycles to crack initiation, N_{fi}, to peak combustor liner temperature, T^*_{mh}, the compressor outlet temperature,T_3, and the von-Mises stress, σ_{vm}. The von Mises, or equivalent stress, is computed based on the following stress scaling by Foltz and Kenworthy [12]. The baseline liner stress σ_{base} and liner temperature T_{base} for each panel are calibrated based on ANSYS and CFD calculations of these parameters for the liner.

$$log(N_{fi}) = g_1({T_{mh}}^*, T_3, \sigma_{vm}) \tag{32}$$

$$\frac{\sigma_{vm}}{\sigma_{base}} = \frac{T_{mh} - T_3}{T_{base} - T_3} \tag{33}$$

Crack propagation is modeled by a response surface equation (Equation 34) that was created by applying a regression analysis to data from the work of Jablonski [13]. $\bar{T}_{mh}$ is the average liner temperature between the slot exit and the end of the liner panel, σ_{ave} is the average equivalent stress corresponding with the average liner temperature, and a is the crack length. This model relates the crack growth rate to the liner temperature and the stress intensity factor, K, where Y is a numerical correction

factor which takes into account the geometry of the panel through which the crack propagates [16].

$$log_{10}(\frac{da}{dN_{fp}}) = g_2(K, \bar{T}_{mh}, T_{base}, \sigma_{base}, T_3) \quad (34)$$

$$K = H\sigma_{ave}\sqrt{\pi a} \quad (35)$$

Integrating Equation 34 over each cup section and panel section increases the computation time by more than one order of magnitude compared to cases where only an algebraic crack initiation model is used. In order to decrease the computation time required for the Monte Carlo Analysis to converge, a response surface was created for a liner with average baseline temperatures and stresses for this combustor (Equation 36), where β_n are the regressors of this polynominal equation.

$$log_{10}N_{fp} = \sum_n \beta_n \bar{T}_{mh}^n \quad (36)$$

4 Model Assessment

The probabilistic model was assessed using available combustor outlet temperature and combustor liner temperature data acquired from rig tests conducted at GE Aircraft Engines. However, these experiments were not designed to assess this probabilistic model. In particular, the wall temperature data do not solely reflect the impact of manufacturing variability. The prohibitive costs associated with duplicating these experiments, however, required the use of the available data for the model assessment.

The combustor outlet temperature data acquisition procedure consisted of a circumferential survey of the outlet plane. A rake with five thermocouples traversed the combustor exit plane in 3.6 degree increments, yielding 500 data points. The combustor annulus was then divided into N regions corresponding with the N cup sections. Then, the data points in each cup section were averaged in order to compute the outlet bulk gas temperature for each cup section. The coefficients of variation of the combustor outlet temperature for the liner wall temperature measurements and the probabilistic model liner temperature estimate are shown in Figure 9. The coefficients of variation are approximately 0.02. These results indicate that the network flow and bulk temperature models yield results that are consistent with the combustor outlet temperature data.

The combustor liner temperature measurements were acquired from thermocouples embedded in and placed on the cold side of the combustor liner walls. The thermocouples were placed in "hot" and "cold" spots previously identified using thermal paint. Although the wall temperature measurements were taken while the combustor was subject to a range of operating conditions, the measurements used in this study were acquired when the combustor conditions were consistent with the sea-level, hot-day operating point. Moreover, the inner diameter and outer diameter wall temperature measurements for each panel were lumped together prior to the statistical analysis due to the small amount of available data.

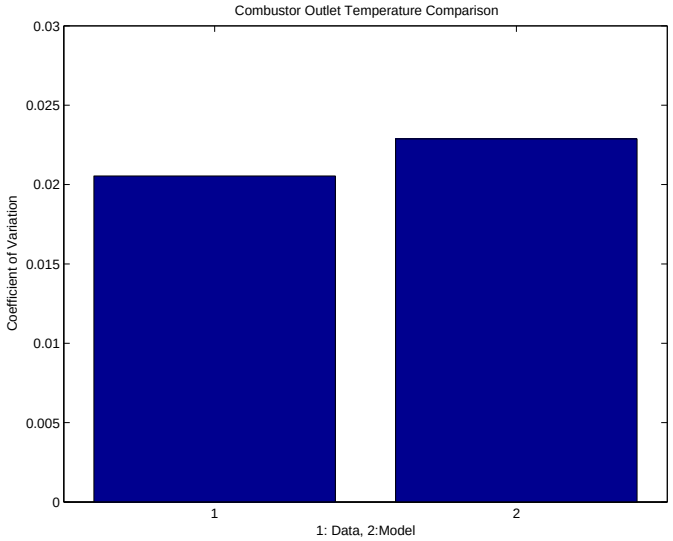

Figure 9. Combustor outlet temperature variability: model vs. experiment

The mean and standard deviation of the temperature difference between the thermocouple measurements and the design temperature (T_{mho}) for each panel were computed and then compared to the model's estimates of these quantities, as shown in Figures 10 and 11. The 95 percent upper and lower confidence bounds for these estimates have also been plotted. The inner and outer diameter statistics were averaged and presented by panel in these figures. The model's estimates of the mean liner temperatures for panels one, two, and four fall outside of the 95 percent confidence bounds of the thermocouple data. The model's mean liner temperature estimate falls within these confidence bounds for the panel three data. The model's estimate of the liner temperature standard deviation matches the lower confidence bound of the data for panels one through four.

The analysis of the wall temperature data yields an overestimate of the effects of manufacturing variability. This combustor contains two different types of metering hole sizes in each panel section, the baseline holes and the preferential holes. The baseline cooling holes are the original design metering holes. After testing reveals elevated temperatures in certain areas, larger pref-

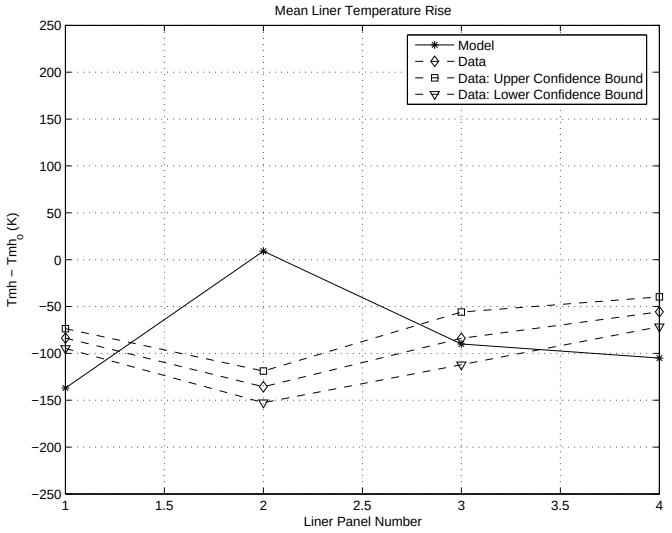

Figure 10. Liner temperature rise by panel

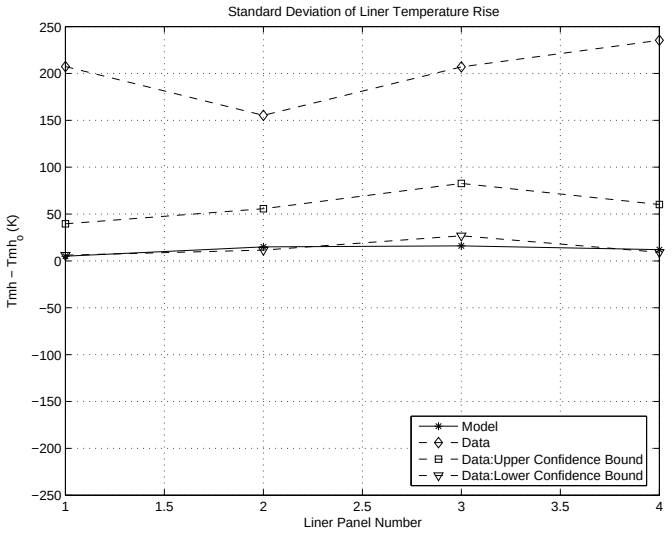

Figure 11. Liner temperature rise variability by panel

erential holes are built into the liner in order to mitigate the high temperature areas. Cooling holes of differing sizes yields a local cooling film effectiveness that varies with circumferential location in a panel section. Furthermore, the thermocouples were not placed in identical circumferential locations relative to the fuel injector for several cup sections. Thus, some thermocouples are placed in front of the baseline cooling wholes while others are located in front of preferential cooling holes. This thermocouple placement results in larger cup-to-cup variability in liner temperature than is caused by manufacturing variability.

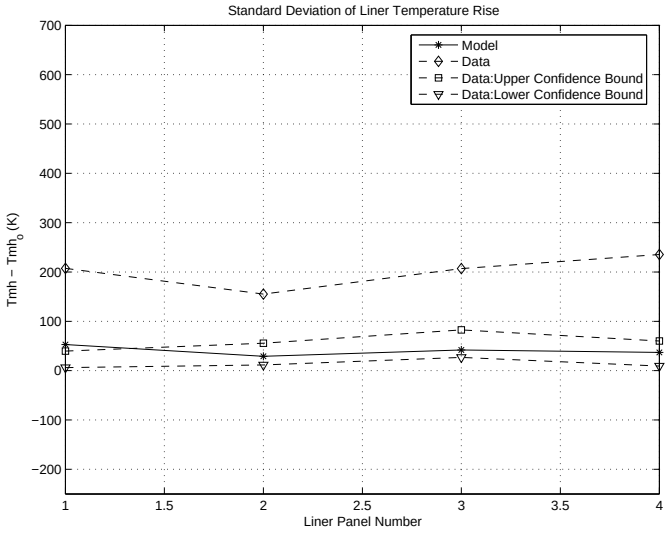

Figure 12. Liner temperature rise variability by panel. Baseline cooling holes modeled.

The thermocouple placement process is modeled as a binomial distribution in order to estimate the effects of the baseline metering holes. The probability of "success" for each trial is equal to the ratio of the number of preferential cooling holes to the total number of holes. Thus, for each "successful" trial, the dilution hole diameter is set equal to the preferential metering hole diameter. Otherwise, the all of the metering hole diameters are reduced by a fraction of the preferential cooling hole diameter. Figure 12 shows that the standard deviation of the combustor liner temperature is more consistent with the variability of the wall temperature data as a result of modeling the effects of the baseline cooling holes.

5 Liner Life Distribution Shift

This probabilistic analysis yields shifts of the peak liner temperature and the combustor liner life distributions. The effect of manufacturing variability is to increase the peak liner temperature in a combustor, which causes a translation of the peak liner temperature distribution. Figure 13 consists of a graph of the difference between the peak liner temperature distribution and the nominal peak temperature normalized by the peak temperature. The figures shows that the average peak temperature is greater than the nominal peak temperature. The peak liner temperature is sensitive to the variability of the input parameters.

The combustor liner life distribution shift occurs because liner life is driven by the maximum liner temperature, and hence, the lowest life panel section. The effect of variability is to increase the difference between the lowest life value and the nominal value for a given combustor such that the combustor liner

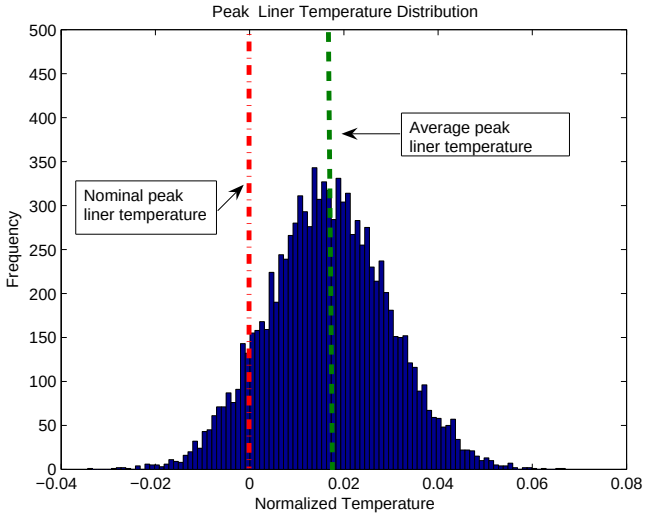

Figure 13. Peak liner temperature distribution

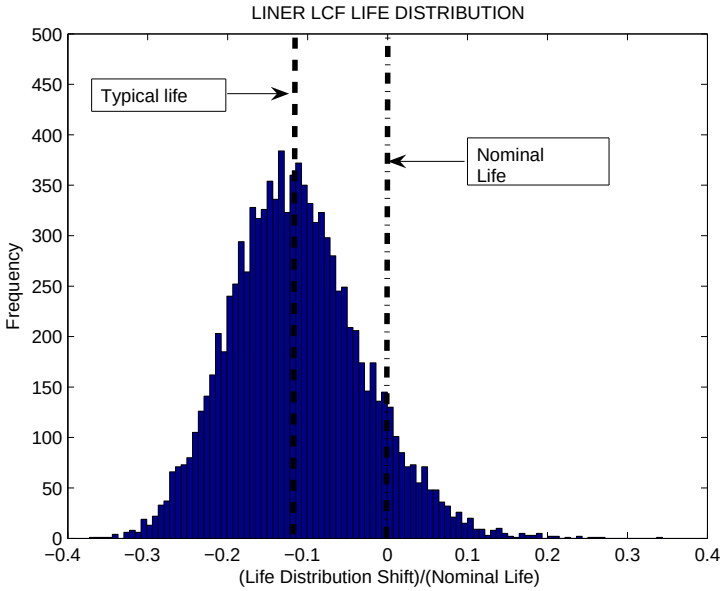

Figure 14. Combustor liner life probability distribution

life distribution has a mean value that is less than the nominal life. Figure 14 consists of a graph of the normalized life distribution, or life distribution minus the nominal life, divided by the nominal life. A value of zero indicates that the mean of the life distribution is equal to the nominal life. This figure, however, shows that the mean normalized liner life is less than the nominal normalized life. In particular, the probability that a combustor's liner life will be less than the nominal life is approximately 90 percent (Figure 15). These results indicate that combustors designed to the nominally calculated life will most likely fail earlier than predicted using deterministic methods.

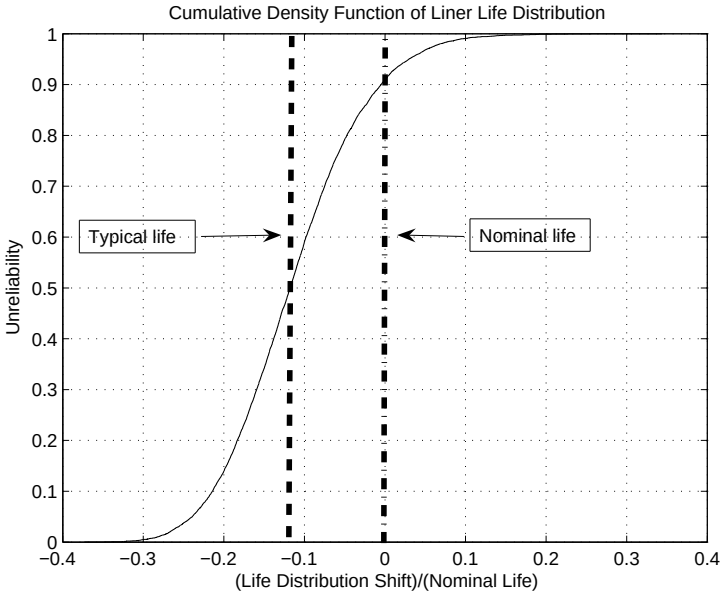

Figure 15. Combustor liner life CDF

6 Sensitivity Analysis

Another use for this probabilistic model is the determination of the key drivers of combustor liner LCF life variability using a sensitivity analysis. First, the random variables and the LCF life response are transformed into standard variables such that

$$\chi_n = \frac{\chi_n - \mu_{\chi_n}}{\sigma_{\chi_n}} \tag{37}$$

and

$$\hat{Y} = \frac{Y - \mu_Y}{\sigma_Y} \tag{38}$$

.

Second, the LCF life response is fitted to the following quadratic, multi-variate response surface equation (39), where $\hat{Y}$ is the standardized random variate for the natural logarithm of combustor liner LCF life ($Y = log(N_f)$), χ_n is the n^{th} random variable input, and N is the number of random variables in the response surface equation. The coefficient of determination (or

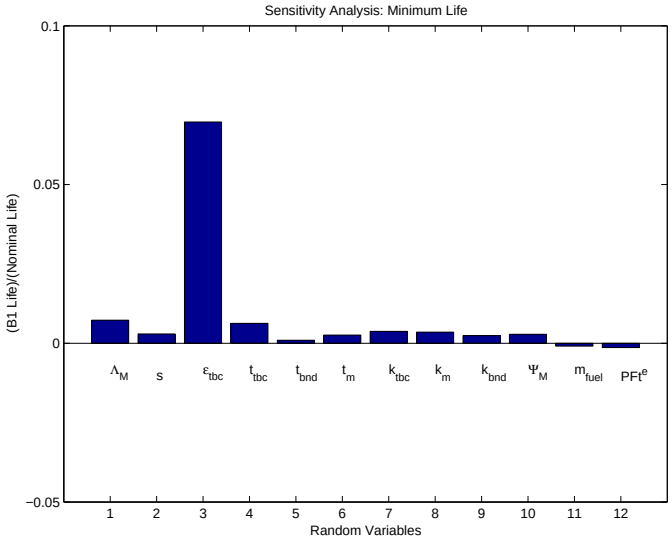

Figure 16. Sensitivity analysis: B1 life changes for 90 percent tolerance reductions.

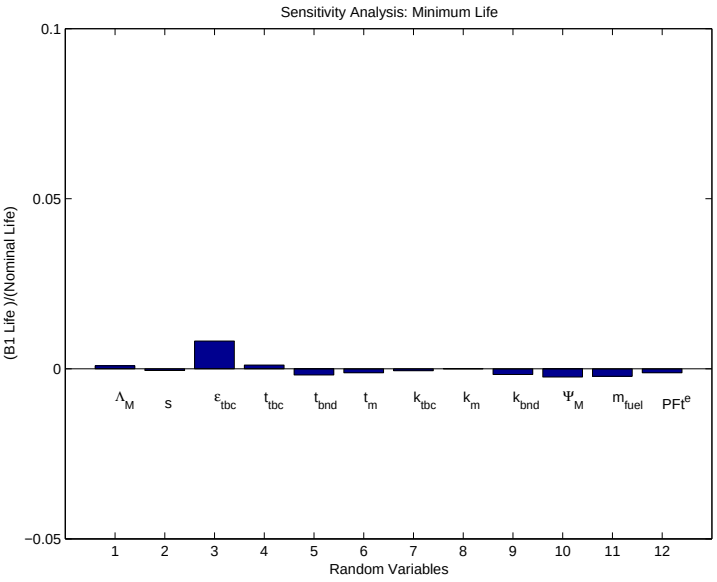

Figure 18. Sensitivity analysis: B1 life for ten percent tolerance reductions.

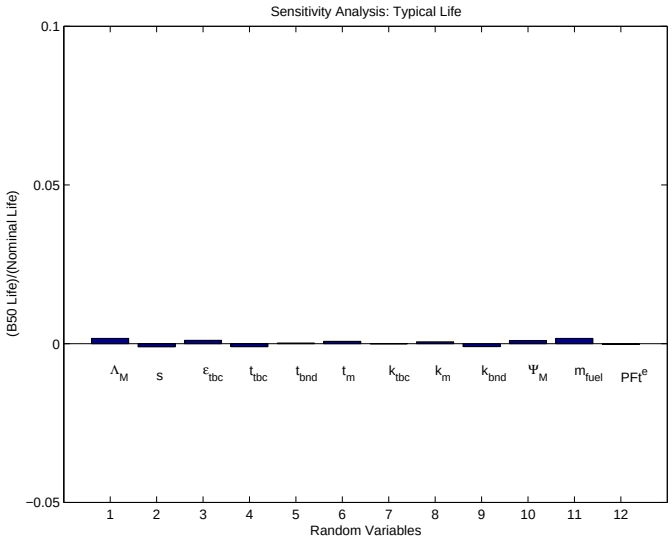

Figure 17. Sensitivity analysis: B50 life changes for 90 percent tolerance reductions.

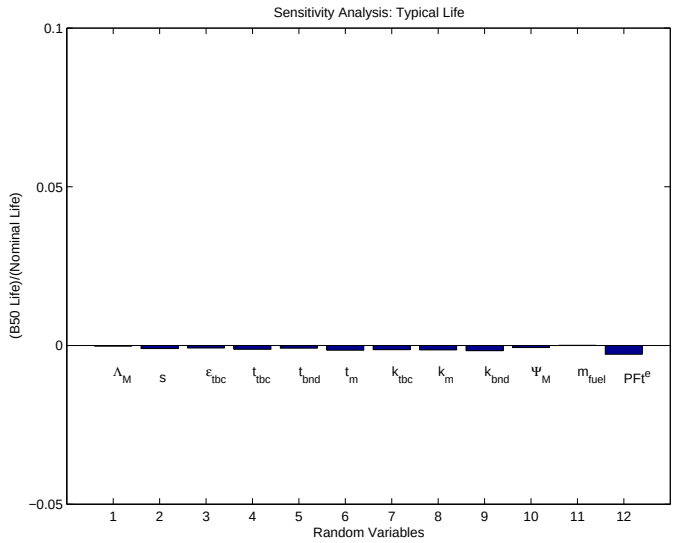

Figure 19. Sensitivity analysis: B50 life for ten percent tolerance reductions.

R^2), which estimates the proportion of variability explained by the response surface equation [20], is approximately 90 percent. Thus, the response surface equation captures most of the modeled variability in the combustor liner life. As a result, the response surface equation is adequate for this sensitivity analysis.

$$\hat{Y} = a_0 + \sum_{n=1}^{N} b_n \chi_n + \sum_{n=1}^{N-1} \sum_{m=n+1}^{N} c_{n,m} \chi_n \chi_m + \sum_{n=1}^{N} d_n {\chi_n}^2 \qquad (39)$$

Third, a one-at-a-time sensitivity analysis was used in or-

der to identify the key drivers of manufacturing variability on combustor liner LCF life. After composing the RSE, the standard deviations of these standardized random variables were decreased by 10 percent and 90 percent in a one-at-a-time fashion while holding the standard deviations of the other parameters to their original settings in order to estimate the impact of changing the manufacturing variability on the minimum or B1 life and the typical or B50 life. 10 percent tolerance reductions represent relatively small changes in the manufacturing tolerances while 90 percent tolerance reductions are considered large changes.

The 90 percent tolerance reductions show that the key driver of the B1 life is the TBC surface emissivity (Figure 16). The B1 life increases by 7 percent of the nominal liner life when the TBC surface emissivity variability is decreased by 90 percent. The TBC emissivity is the key driver of LCF life variability for this combustor because the radiative load contribution dominates that of the convective load to panel 2. As a result, the liner heat load is sensitive to variations in the radiative load caused by the TBC surface emissivity variation. Furthermore, the TBC surface emissivity coefficient of variation is the greatest of the set of 12 random variables presented in this paper.

The ten percent tolerance reductions also show that the TBC surface emissivity is the key driver of liner life variability. However, the B1 life only increases by approximately one percent of the nominal liner life (Figure 18). Furthermore, this sensitivity study also shows that the B50 life is insensitive to manufacturing tolerance reductions for both cases (Figures 17, 19). Overall, these results indicate that one-at-a-time tolerance reductions do not significantly impact the probability of half of the combustor liners failing while the probability that 1 percent of the combustors will fail is significantly impacted by tightening the TBC surface emissivity tolerance.

7 Flame Luminosity Factor Impact

Higher fidelity analysis of the combustor flow field shows that the flame is located in the region corresponding with the end of the panel one section and the beginning of the panel two section as measured longitudinally from the fuel injectors. Our heat transfer analysis, however, is performed on the portion of liner near the end of each panel. The combustion gas in the panel two region does not contain the flame. Within the scope of the 1-D heat transfer model, we can assume that the radiative heat flux is dependent on a nonluminous flame. In order to model this effect, the flame luminosity factor was reduced from approximately 1.7 to 1.0 for the panel two.

This modification of the liner heat transfer model resulted in several changes. First, the liner temperature rise for panel two decreased (Figure 20) while the liner temperature rise variability remains unchanged (Figure 21). Figure 22 shows that the model's estimate of the liner temperature variability is more consistent with the thermocouple data when the impact the baseline

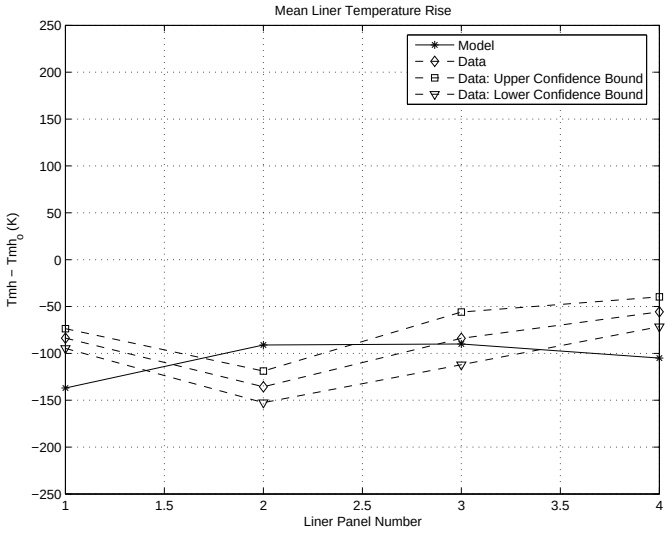

Figure 20. Liner temperature rise by panel

cooling holes is taken into account. The mean liner temperature rise estimate for panel two is more consistent with the TC data than the previous results. Second, the liner life distribution shift increased relative to the previous case. Overall, the typical life increases as a result of the decreased flame luminosity factor for panel two but the distribution shift increases by a factor of three (Figures 24, 25). Also, these results show that the probability that most of the liner lives will be below the nominally predicted life is greater than 99 percent. Finally, the regression analysis yields a coefficient of determination that is approximately 0.4. This poor fit implies that the response surface for liner LCF life does not capture all of the variability in the Monte Carlo data. As a result, this response surface methodology cannot be used to identify the key driver of the minimum liner life. These results do underscore, however, the significant impact of the radiative load on the overall life distribution.

8 Summary and Conclusions

This paper has introduced a probabilistic modeling methodology for estimating the impact of manufacturing variability on combustor liner temperature and LCF life. The model estimates the cup-to-cup variability of the combustor outlet gas temperature consistent with the experimental data for the combustor that we have analyzed. A comparison of the combustor wall temperature measurements and the model shows that the model underestimates the cup-to-cup liner temperature variability. However, the high variability shown in the data is driven by the impact of two types of metering holes on the film effectiveness and, ultimately, the liner temperature. Furthermore, we have also shown that there is a fundamental liner life distribution shift. The proba-

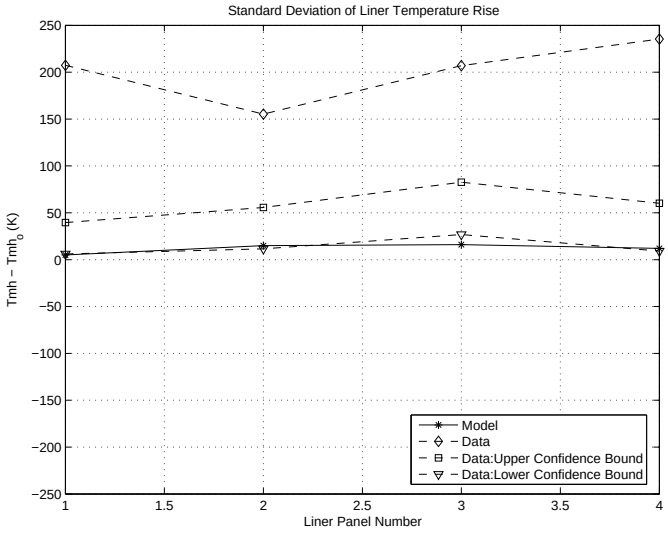

Figure 21. Liner temperature rise variability by panel

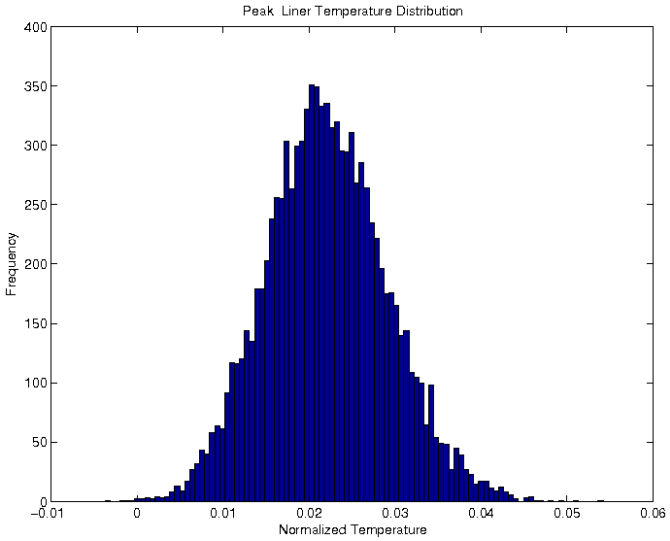

Figure 23. Liner temperature rise by panel (modified luminosity factor)

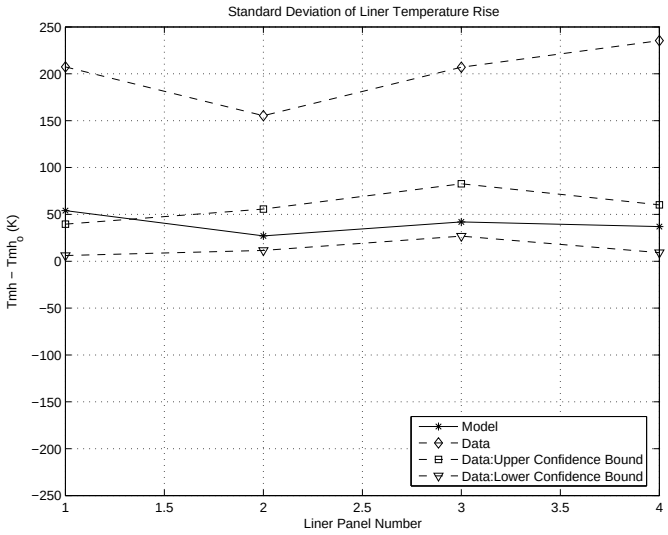

Figure 22. Liner temperature rise variability by panel. Baseline cooling hole effects included.

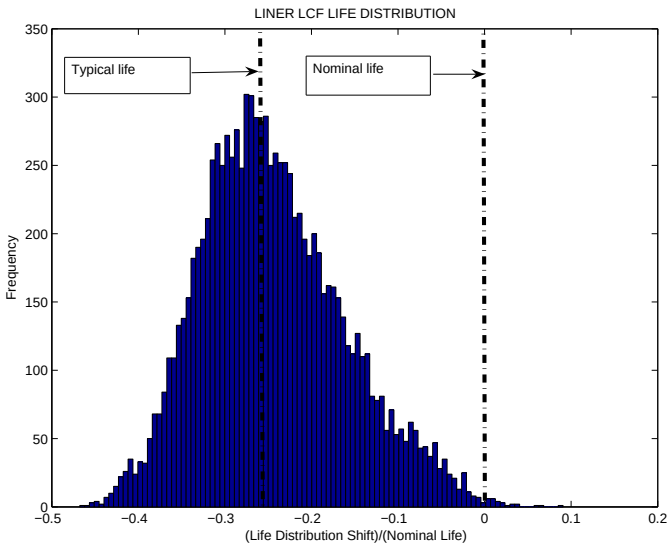

Figure 24. Liner life distribution (modified luminosity factor)

bility that the liner life for a randomly selected combustor is less than the nominal life is approximately 90 percent. In addition, a sensitivity analysis also identifies the key driver of the B1 life to be the TBC surface emissivity. The B50 life is shown to be relatively insensitive to these tolerance changes. Reducing the TBC surface emissivity variation will increase the minimum life for a fleet of combustors while the number of cycles for half of the fleet to fail will remain approximately unchanged.

Identification of the key drivers of minimum liner life and the magnitude of the liner life distribution shift is dependent on the levels of the manufacturing variability assumed in the model and on the accuracy of the nominal liner temperature estimates. In the model, the panel two liner temperatures drive the overall peak liner temperatures in the combustor. A combination of high radiative loads relative to convective loads for panel two and high percent variation of the TBC emissivity resulted in the TBC emissivity being the key driver of the B1 life. However, the thermocouple data show that the panel two temperatures are not the peak liner temperatures for this combustor. Improved accuracy

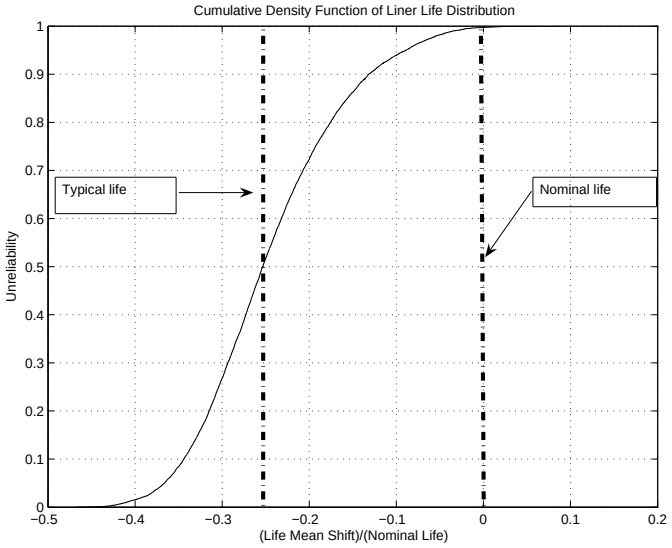

Figure 25. Liner life CDF (modified luminosity factor)

of the deterministic models may yield a different driver of the B1 life. Moreover, combustors with input parameters containing different levels of variability than the parameters presented in this paper may also yield different estimates for the liner life mean shift. Furthermore, the B1 life may be most sensitive to a parameter other than the TBC surface emissivity for convection dominated liners.

9 Future Work

There are several additional features that are needed in order to more accurately estimate the combustor liner life variability consistent with the field data and to assess the key drivers of the mean and variance of liner life. First, the underlying reasons for the poor response surface fit to the Monte Carlo data in the second case should be understood. Solving this problem will lead to a general methodology for identifying the key drivers of the liner life using a one-at-a-time sensitivity analysis. Second, the impact of operational variability on combustor liner life should be assessed by modeling the variability of atmospheric conditions such as ambient temperature, pressure, and percent relative humidity and then propagating these effects through the probabilistic model. Third, models which relate manufacturing variability to combustor unmixedness would improve the estimates of the near wall gas temperature variability. Fourth, models for the dilution jet-cooling film interaction would improve estimates of the flame side liner convection heat flux near the dilution holes. Finally, the inclusion of simplified liner life models which accurately estimate the first order effects of creep and oxidation would increase the accuracy of the combustor liner life distribution estimate.

Acknowledgements

The authors would like to acknowledge the funding provided by the MIT Department of Aeronautics and Astronautics and the Ford Foundation. We would also like to thank Harris Abramson, Aureen Currin, and John Starkweather of GE Aircraft Engines for providing us with the experimental and numerical data that were used to assess our model and for the time spent reviewing this paper.

REFERENCES

[1] Aurthur Lefebvre. *Gas Turbine Combustion.* Taylor Francis. 1999.

[2] W.J. Dodds and D.W. Bahr. Combustion System Design. Notes.

[3] Victor E. Garzon and David L. Darmofal. *Impact of Geometric Variability in Axial Compressor Performance.* Transactions of the ASME. Vol. 125, October 2003.

[4] Vince Sidwell and David L. Darmofal. *A Selective Assembly Method to Reduce The Impact of Blade Flow Variability on Turbine Life.* Proceedings of 2004 ASME Turbo Expo, Vienna, Austria. Paper No. 2004-53581.

[5] Caroline Lamb and David L. Darmofal. *Performance-based Geometric Tolerancing of Compressor Blades.* Proceedings of 2004 ASME Turbo Expo., Vienna, Austria, Paper No. 2004-53592.

[6] Dmitri Mavris and Bryce Roth. *A Methodology For Robust Design of Impingement Cooled HSCT Combustor Liners.* AIAA 1997.

[7] M. A. Mawid et al. *Development and Validation of Detailed and Reduced Chemical Kinetic Mechanisms for Oxidation of JP-8/Jet-A/JP-7 Fuels.* ISABE-2003-1028.

[8] P. Gosselin, A de Champlain, and D. Kreschmer. *Prediction of Wall Heat Transfer for a Gas Turbine Combustor.* Proc. Instn. Mech. Engrs. Vol. 213, Part A, 1999.

[9] Joseph Monty. Personal communication. GE Aircraft Engines. 2003.

[10] Warren M. Rohsenow, et. al. *Handbook of Heat Transfer.* Third Edition. McGraw-Hill Handbooks. 1998.

[11] Alfredo Ang and Wilson Tang. Probability Concepts in Engineering Planning and Design: Volume I - Basic Principles. John Wiley Sons, Inc. 1975.

[12] H.L. Foltz and M.J. Kenworthy. *A Procedure for Evaluating Fuel Composition Effects on Combustor Life.* 82-GT-296.

[13] D.A. Jablonski. *Fatigue Behavior of Hastelloy-X at Elevated Temperatures in Air, Vacuum, and Oxygen Environments.* MIT Ph.D. Thesis. Department of Materials Science and Engineering. 1978.

[14] Michael F. Modest. *Radiative Heat Transfer.* McGraw Hill, 1999.
[15] A.F. Mills. *Basic Heat Mass Transfer, Second Edition.* Prentice Hall, Inc. 1999.
[16] Michael F. Ashby and David R.H. Jones. *Engineering Materials I: An Introduction To Their Properties Applications.* Second Edition. Butterworth-Heinemann.
[17] Steve Stephens and Mark Shaw. Personal communication. GE Aircraft Engines. 2004.
[18] Austin Mascarenas. Personal communication. Delta Airlines. 2004.
[19] Aureen Currin. Personal communication. GE Aircraft Engines. 2004.
[20] Douglas C. Montgomery. *Design and Analysis of Experiments: Second Edition.* John Wiley Sons. 1984.